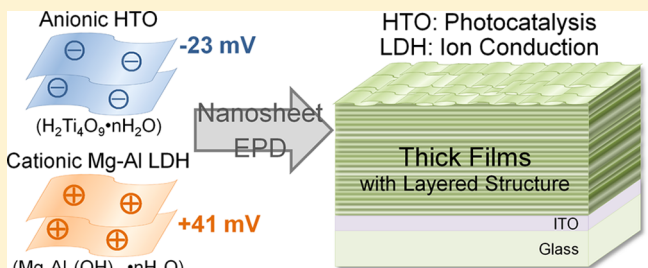


# Characterization and Film Properties of Electrophoretically Deposited Nanosheets of Anionic Titanate and Cationic MgAl-Layered Double Hydroxide

Atsunori Matsuda,\* Hisatoshi Sakamoto, Mohd Arif Bin Mohd Nor, Go Kawamura, and Hiroyuki Muto

Department of Electrical and Electronic Information Engineering, Toyohashi University of Technology, 1-1 Hibarigaoka, Tempaku, Toyohashi, Aichi 441-8580, Japan

**ABSTRACT:** Anionic hydrated titanate ( $H_nTiO_m$ : HTO) nanosheets and cationic magnesium–aluminum layered double hydroxide (Mg–Al LDH) nanosheets were electrophoretically deposited on positively and negatively charged indium tin oxide (ITO)-coated glass substrates, respectively. The HTO nanosheets and Mg–Al LDH nanosheets obtained were identified in neutral water as  $H_2Ti_4O_9 \cdot nH_2O$  with a  $\zeta$ -potential of  $-23$  mV and  $Mg_6Al_2(OH)_{18} \cdot 4.5H_2O$  with a  $\zeta$ -potential of  $+41$  mV, respectively. Dense and smooth HTO and Mg–Al LDH films with layered structures with thicknesses of about  $10\text{--}15\ \mu\text{m}$  were prepared in  $300\text{ s}$  at  $7.5\text{ V}$  by electrophoretic deposition (EPD) from the nanosheet suspensions. Both EPD HTO and LDH films showed elasticity because of their layered laminate structures. The HTO thick films demonstrated large adsorption properties and high photocatalytic activity, while the Mg–Al LDH thick films showed relatively high ionic conductivity of  $10^{-5}\text{ S cm}^{-1}$  at  $80\text{ }^\circ\text{C}$  and  $80\%$  relative humidity.



## INTRODUCTION

Electrophoretic deposition (EPD) is a simple and cost-effective process that enables us to obtain uniform thick films under ambient pressure and temperature in comparison with conventional physical vapor deposition (PVD) using vacuum system and aerosol deposition (AED) using high-pressure carrier gas. This technique can be widely applied to produce coatings for substrates for use as electrodes of various shapes and allows us to produce laminated composite materials composed of ceramics, polymers, dyes, and metals.<sup>1–3</sup> EPD is an effective method to prepare nanostructured thick films of more than  $1\ \mu\text{m}$  in thickness and has been widely used for the fabrication of functional coatings of charged colloidal materials such as nanoparticles, nanotubes, and nanosheets.<sup>4–6</sup> When we use nanosheets for EPD, the resulting EPD films consisting of the nanosheet materials may show better adhesion without cracking in the films when compared with EPD films based on particles. Various types of two-dimensional nanosheets have been synthesized by ion exchange and delamination of layered alkali titanates, layered double hydroxides, layered niobates, and  $\alpha$ -zirconium phosphate.<sup>7–10</sup>

Hydrated titanate (HTO) nanosheets show high photocatalytic activity, distinctive solid acidity, good ion exchange properties, and large intercalation capacity because of their high specific surface area, high activity, and ultrathin dimensions. The synthesis, structures, and characteristics of several types of nanosheets derived from HTOS such as  $H_2Ti_3O_7$ ,  $H_2Ti_4O_9$ , and  $H_2Ti_5O_{11}$  have been reported.<sup>11–13</sup> Thin flakes and porous aggregates of HTO can be obtained from colloidal nanosheet suspensions by centrifugation and drying, whereas the

immobilization of HTO nanosheets on substrates, that is, the formation of thin or thick films of these HTO nanosheets on substrates, is essential for practical applications. For the EPD of HTO, highly oriented titania nanosheet films were prepared on Pt substrates under optimal conditions.<sup>14</sup> An interesting UV-visible light-sensitive energy conversion system design using methyl viologen-intercalated titania nanosheet films prepared by EPD on indium tin oxide (ITO)-coated glass substrates has been reported.<sup>15</sup> We have also reported the preparation of layered thick films from a surface-modified HTO ( $H_2Ti_4O_9$ ) nanosheet colloidal suspension by EPD.<sup>16</sup> The  $H_2Ti_4O_9$  nanosheet is composed of corrugated ribbons of edge-sharing  $TiO_6$  octahedral units, which join at the corners to form stepped sheets separated by  $H^+$  ions in an intersheet.

Layered double hydroxides (LDHs) have attracted considerable attention for applications including catalysts, adsorbent materials and inorganic fillers for organic–inorganic composites. Several types of LDH, including so-called hydrotalcite clays such as Mg–Al LDH, Zn–Al LDH, and Co–Al LDH, have been reported.<sup>8,17,18</sup> Among these materials, Mg–Al LDH and its nanosheets were found to be promising as a solid electrolyte for direct methanol fuel cells to prevent methanol crossover.<sup>19–21</sup> For the EPD of Mg–Al LDH, oriented films were fabricated on aluminum substrates and were used to

## Special Issue: Electrophoretic Deposition

Received: July 2, 2012

Revised: November 13, 2012

Published: December 3, 2012

remove heavy metal ions and anionic dyes from aqueous solutions.<sup>22</sup> A novel controlled molecular release based on highly oriented LDH nanoplates on ITO/glass substrates was also reported.<sup>23</sup>

In the present study, film formation using negatively charged HTO nanosheets and positively charged Mg-Al LDH nanosheets in water by EPD has been investigated and the structures of the resulting EPD nanosheet films have been evaluated. The mechanical properties of the EPD nanosheet films have also been evaluated and compared using a nanoindentation system. In addition, the photocatalytic activity and ionic conductivity of these EPD nanosheet films have been discussed.

## EXPERIMENTAL SECTION

**Electrophoretic Deposition.** An HTO colloidal suspension consisting of tetratitanate ( $H_2Ti_4O_9$ ) nanosheets (2.6 wt %, pH = 7.6) was supplied by Otsuka Chemical Co., Ltd., Osaka, Japan. The HTO suspension was prepared from layered titanates by exfoliation using *N,N*-dimethylmethylethanolamine (DMEA), which was then neutralized with boric acid and washed with deionized water (this process is the subject of Japanese Unexamined Patent Application Publication No. P2009-161678). The layered titanate was synthesized from  $TiO_2$ ,  $K_2CO_3$ , KCl, and LiOH at 1020 °C and was treated with 10% sulfuric acid. The layered titanate obtained was then dispersed in 3.5% hydrochloric acid, filtrated, and repeatedly washed with pure water before the exfoliation process using DMEA. A colloidal suspension of Mg-Al LDH acetate nanosheets (1.0 wt %, pH = 9.8) was supplied by Tayca Co., Osaka, Japan. The Mg-Al LDH nanosheets were prepared from hydrotalcite in a  $Mg(CH_3COO)_2$  aqueous solution. The Mg-Al LDH nanosheets obtained were separated by centrifugation, dried at 90 °C, pulverized, and then dispersed in pure water (this process is the subject of Japanese Unexamined Patent Application Publication No. P2006-274385). The thicknesses of the HTO and Mg-Al LDH nanosheets were measured using an atomic force microscope (AFM, NPX 200, SII Nano Technology Inc.). The surface charges of the HTO and Mg-Al LDH nanosheets in deionized water were measured using a  $\zeta$ -potential analyzer (ELS-Z1NS, Otsuka Electronics Co., Ltd.). An average of five measurements at the stationary level was taken for each point.

ITO-coated glass substrates (<7 Ω/◻) were used as the counter and working electrodes for deposition. The distance between the facing ITO-coated glass substrates was fixed at 1 cm. The anionic HTO and cationic Mg-Al LDH nanosheets were electrophoretically deposited on the positively and negatively charged ITO-coated glass substrates, respectively. The applied voltage was maintained using a potentiostat/galvanostat (SI1287, Solartron) at 7.5 V DC and the deposition time for electrophoresis was adjusted in a range from 50 to 300 s. During EPD of the HTO and LDH nanosheets, changes in the current densities were also measured using the potentiostat/galvanostat. After EPD, the films were dried at room temperature overnight.

**Evaluation of Film Properties.** The microstructures of the EPD films were observed using a scanning electron microscope (S-4800, Hitachi High-Tec., Co., Ltd.) and an X-ray diffractometer (RINT 2000, Rigaku Co., Ltd.).

Nanoindentation tests were performed at room temperature in an ambient atmosphere, using a specially designed nanoindentation apparatus to measure the hardness of the

EPD films. The penetration of a Berkovich indenter (radius,  $R = 50 \mu m$ ) was controlled to be less than 10% of the film thickness using a piezo actuator. The resolution for control of the penetration depth via the piezo actuator was 0.04 nm. The penetration depth  $h$  was measured using twin capacitive gap sensors and the indentation load  $P$  was monitored using a load cell. The indentation tests were conducted on the EPD films on ITO-coated glass substrates at a penetration rate of 50 nm/s.

The indentation contact behavior was well characterized by the load  $P$  versus penetration depth  $h$  hysteresis during the loading and subsequent unloading processes. The relationship between the indentation load  $P$  and  $h$  is expressed by

$$P = k_1 h^2 \quad (1)$$

where  $k_1$  is a constant. The relative residual depth  $\xi_r$  was defined by the depth of the residual impression  $h_r$  normalized relative to the maximum penetration  $h_{max}$  as

$$\xi_r = h_r / h_{max} \quad (2)$$

which is an elastoplastic material parameter that is independent of both  $P_{max}$  and  $h_{max}$ . As a geometrical parameter for characterization of the contact periphery between the indenter and the indented material surface at the peak load, the surface profile parameter  $\gamma_1$  is defined by the ratio of  $h_{max}$  to  $h_c$  using the contact depth  $h_c$  induced at  $P_{max}$ . The correlation between  $\gamma_1$  and  $\xi_r$  is represented by the following empirical formula:

$$\gamma_1 = \frac{\pi}{2} (1 - 0.43 \sqrt{\xi_r}) \quad (3)$$

The Meyer hardness  $H_M$  is conventionally defined as the ratio of the peak load,  $P_{max}$ , to the projected area,  $A_r$ , of the residual indentation impression. Using the approximation of  $A_r \approx A_c$ , where  $A_c$  is the projected contact area, an alternative expression for the Meyer hardness is given by

$$H_M(k_1) = \frac{P_{max}}{A_c} = \frac{P_{max}}{gh_c^2} = \frac{\gamma_1^2}{g} k_1 \quad (4)$$

where the geometrical factor  $g$  is 24.5 for the Berkovich indenter and is related to the inclined face angle  $\beta$  of the indenter by  $3\sqrt{3} \cot^2 \beta$ . The Meyer hardness value can be calculated using eq 4 and  $\gamma_1$  in eq 1 using the  $\xi_r$  value that was obtained experimentally.<sup>24–27</sup> The mechanical properties of soda-lime (SL) glass and poly(methyl methacrylate) (PMMA) were also evaluated through nanoindentation tests under the same conditions for comparison. The practical scratch resistance of the EPD films was also evaluated at room temperature in an ambient atmosphere on the basis of the pencil hardness test (JIS KS600-5-4, ISO15184, ASTM D3363).

The adsorption properties and photocatalytic activity of the HTO nanosheet films were evaluated using a  $10^{-5}$  M methylene blue (MB) aqueous solution as an indicator. The MB aqueous solution (10 mL) was poured into a Petri dish, and the HTO nanosheet films on the ITO-coated glass substrates were soaked in the MB solution. For the evaluation of the adsorption properties, the substrates with films were submerged in the MB solution for soaking times from 30 to 180 min, extracted from the solution, and then dried by blowing nitrogen gas on them. The MB absorbance of the dried films was measured in an ambient atmosphere by UV-vis spectroscopy (V-560, Jasco, Japan). To evaluate the photocatalytic activity, the MB-adsorbed films that were soaked for 180 min

were UV-irradiated using a black light (illumination intensity of  $1.0 \text{ mW/cm}^2$ ) for a given irradiation time. The changes in the absorbance of the films after UV irradiation were measured using the UV-vis spectrophotometer.

The ionic conductivities of the HTO and Mg-Al LDH nanosheet films were determined from Nyquist plots by an AC method using an impedance analyzer (1260, Solartron) with frequencies ranging from 10 MHz to 1 Hz. The ITO-coated glass substrate and an evaporated gold thin film ( $10 \times 10 \text{ mm}$ ) were used as electrodes for measurements in the thickness direction. The temperature dependence of the conductivity was measured from 30 to 80 °C at a relative humidity (RH) of 80% in air, and the humidity dependence from 50 to 90% RH was measured at 30 °C. The ionic conductivities of pelletized disk samples (10 mm in diameter and 1 mm in thickness) of commercially available hydrotalcite powders (Wako Chemical) were also evaluated for comparison. Prior to proton conductivity measurement of the powders, pelletized samples were prepared by pressing at a loading pressure of 60 MPa for 10 min. During the pelletization, two sheets of carbon paper were placed on both sides of the sample as the electrodes. Proton conductivity was evaluated by AC impedance spectroscopy over a frequency range of 10 MHz to 1 Hz using a system. The measurement conditions were controlled using a temperature- and humidity-controlled chamber (SD-01, ETAC).

## RESULTS AND DISCUSSION

### Characterization of HTO and Mg-Al LDH Nanosheets.

The thickness and size of the HTO nanosheets were estimated to be approximately 1 nm and 10 μm, respectively, from AFM observations, while those of the Mg-Al LDH nanosheets were estimated to be approximately 3–8 nm and 50 μm, respectively. These results suggest that the HTO nanosheets are composed of a monolayer of  $\text{TiO}_6$  units, whereas the Mg-Al LDH nanosheets are composed of aggregates of  $[\text{Mg}-\text{Al}(\text{OH})_2]$  layers. The  $\zeta$ -potentials of the HTO nanosheet and the Mg-Al LDH nanosheet were estimated to be  $-23 \text{ mV}$  and  $+41 \text{ mV}$  in water, respectively.

**Film Formation of Nanosheets by EPD.** The physical appearances of the HTO and Mg-Al LDH nanosheet films are shown in Figure 1. Both nanosheets were deposited smoothly on the ITO-coated glass substrates by EPD under potentiostatic conditions at 7.5 V for 100 s. The HTO film was a translucent white, whereas the Mg-Al LDH nanosheet film was an opaque ash color. No cracks or domed hollows were observed in any of the EPD films. Figure 2 shows cross-sectional and surficial SEM images of the HTO nanosheet films. The HTO nanosheet film thickness increased with increasing EPD time. The EPD HTO film thicknesses obtained after EPD times of 100, 150, and 200 s were about 3.0, 4.5, and 6.0 μm, respectively. The HTO nanosheets were stacked to form a dense film. Shriveled domains were observed on the surface in patches. Figure 3 shows the cross-sectional and surficial SEM images of the Mg-Al LDH nanosheet films. The Mg-Al LDH nanosheet film thickness also increased with increasing EPD time. The EPD LDH film thicknesses obtained after EPD times of 100, 200, and 300 s were 7.0, 10.0, and 14.0 μm, respectively. The electrophoretically deposited Mg-Al LDH nanosheet film also shows dense stacking and a smooth surface. In both the HTO and Mg-Al LDH nanosheet films, few defects, such as domes and hollows caused by  $\text{O}_2$  or  $\text{H}_2$  gas generation at the electrode surfaces, were observed. Also, it can be seen that the HTO nanosheet film surface is smoother than

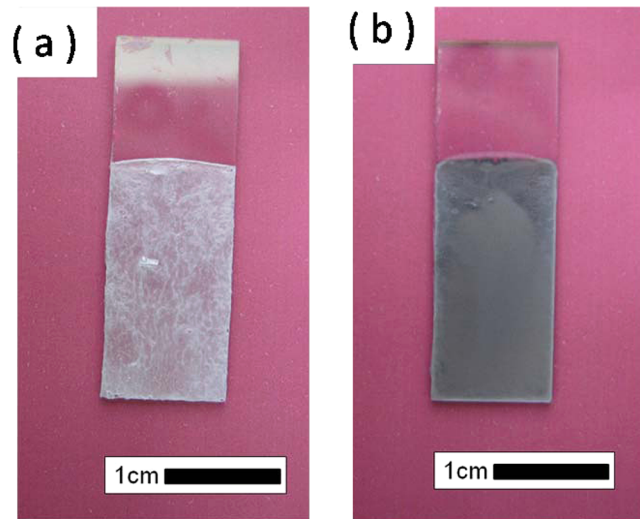


**Figure 1.** Photographs of (a) the HTO nanosheet film and (b) the Mg-Al LDH nanosheet film formed on ITO-coated glass substrates by EPD at 7.5 V for 100 s.

that of the Mg-Al LDH nanosheet film, whereas the cross section of the Mg-Al LDH nanosheet films seems to be denser than that of the HTO nanosheet films. These differences can be ascribed to the monolayer structure (1 nm thickness and 10 μm size) of the HTO nanosheet and the aggregated structure (3–8 nm thickness and 50 μm size) of the Mg-Al LDH nanosheets, as confirmed by AFM observation.

The changes in the EPD film thickness with deposition time at 7.5 V are shown in Figure 4. The thickness of each film was evaluated using cross-sectional SEM at the center of the nanosheet films. A representative single sample for given EPD conditions was adopted for measurement of the film thickness. Open circles and triangles are used to indicate the HTO and Mg-Al LDH films, respectively. Linear relationships between the film thickness and the deposition time were observed for both EPD films. The film thickness reached 10 μm for the HTO nanosheets, and 14 μm for the Mg-Al LDH nanosheets after deposition for 300 s. The HTO nanosheets used have a smaller  $\zeta$ -potential ( $-23 \text{ mV}$ ) than that of the Mg-Al LDH nanosheets ( $+41 \text{ mV}$ ). According to the Helmholtz-Smoluchowski equation, the steady rate of the particles in the colloidal suspension is proportional to both the dielectric constant and the  $\zeta$ -potential. Therefore, the larger  $\zeta$ -potential of the Mg-Al LDH nanosheet has probably resulted in a higher deposition rate.

Changes in the current densities under potentiostatic conditions at 7.5 V for EPD using aqueous suspensions of the HTO and Mg-Al LDH nanosheets are shown in Figure 5. During EPD, the LDH nanosheets show a higher current density than the HTO nanosheets, which can be ascribed to the higher pH value of 9.8 of the LDH suspension compared with a pH value of 7.6 for the HTO suspension. A dramatic decrease in the current density was observed for the LDH nanosheets, which suggests a large increase in the resistivity of the LDH nanosheet films deposited on the ITO/glass substrate. The higher current density during EPD and the larger subsequent decrease in the current density of the LDH nanosheets in comparison with those of the HTO nanosheets probably correspond to the high deposition rate with a high pH value

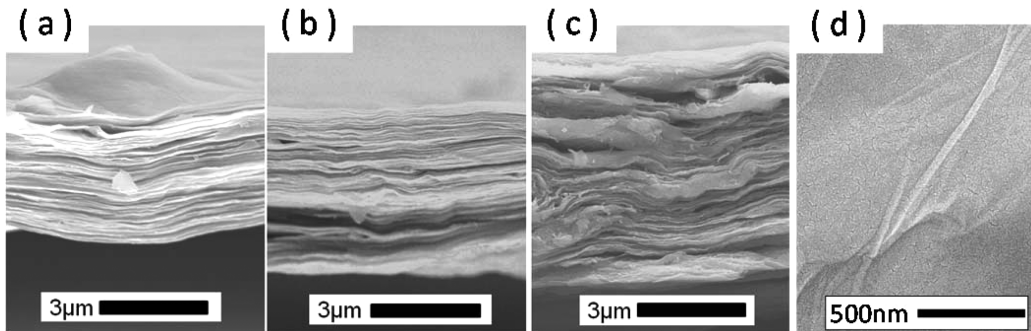


**Figure 2.** Cross-sectional SEM images of HTO nanosheet films formed on ITO-coated glass substrates by EPD under potentiostatic conditions at 7.5 V for (a) 100, (b) 150, and (c) 200 s. (d) Surface images of the HTO nanosheet film formed at 7.5 V for 200 s.

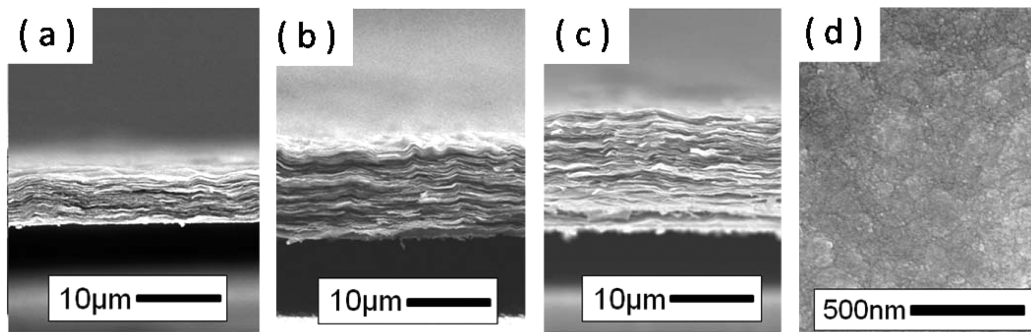


**Figure 3.** Cross-sectional SEM images of Mg-Al LDH nanosheet films formed on ITO-coated glass substrates by EPD under potentiostatic conditions at 7.5 V for (a) 100 s, (b) 200 s and (c) 300 s. (d) Surface images of the Mg-Al LDH nanosheet film formed at 7.5 V for 200 s.

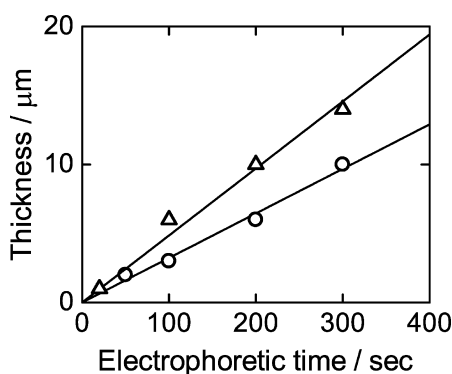


**Figure 4.** Relationship between film thickness and deposition time under potentiostatic conditions at 7.5 V for the nanosheet films. Open circles and open triangles indicate the HTO nanosheet and the Mg-Al LDH nanosheet, respectively.

and the dense structure of the resulting EPD LDH films, respectively.

**Film Properties.** Figure 6 shows XRD patterns for the HTO nanosheet film and the Mg-Al LDH nanosheet film prepared by EPD at 7.5 V for 100 s. The HTO and Mg-Al LDH in the EPD films were identified as tetratitanate ( $\text{H}_2\text{Ti}_4\text{O}_9 \cdot n\text{H}_2\text{O}$ ) and magnesium–aluminum hydroxide hydrate ( $\text{Mg}_6\text{Al}_2(\text{OH})_{18} \cdot 4.5\text{H}_2\text{O}$ ), respectively, which agreed with the compositions of the nanosheets in the suspensions used for EPD. In the XRD patterns of the HTO film shown in Figure 6a, a large diffraction peak is observed at  $8.48^\circ$ , which corresponds to  $d$ -spacing of 1.04 nm between (200) planes. On the other hand, in those of Mg-Al LDH film in Figure 6b, a large diffraction peak is observed at  $11.14^\circ$  corresponding to  $d$ -spacing of 0.79 nm between (003) planes. It can be seen that

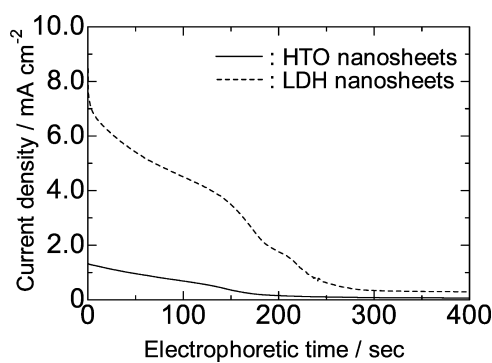


**Figure 5.** Variations in current densities under potentiostatic conditions at 7.5 V for EPD. The solid and broken lines indicate the aqueous suspensions of the HTO and Mg-Al LDH nanosheets, respectively.

the HTO nanosheet film shows higher crystallinity than the Mg-Al LDH nanosheet film. These results indicate that no degradation and no redox reactions occurred in the HTO and LDH nanosheets during EPD under the stated conditions.

Figure 7a and b show typical load–displacement ( $P-h$ ) curves for the EPD HTO and LDH films, respectively. Both films were deposited on ITO-coated glass substrates at 7.5 V for 300 s. The solid curves represent the quadratic relationship of  $P = k_1 h^2$  corresponding to eq 1. For the HTO film, a declination of the measurement plots relative to the quadratic relationship is observed at around 0.6  $\mu\text{m}$ , suggesting the collapse of the HTO film and peeling of the HTO nanosheets. For the LDH film, however, good correspondence between the measurement plots and the quadratic relationship is observed to a penetration depth of 1  $\mu\text{m}$ , indicating that the LDH film deforms elastically in this region. From these  $P-h$  curves, the Meyer hardness

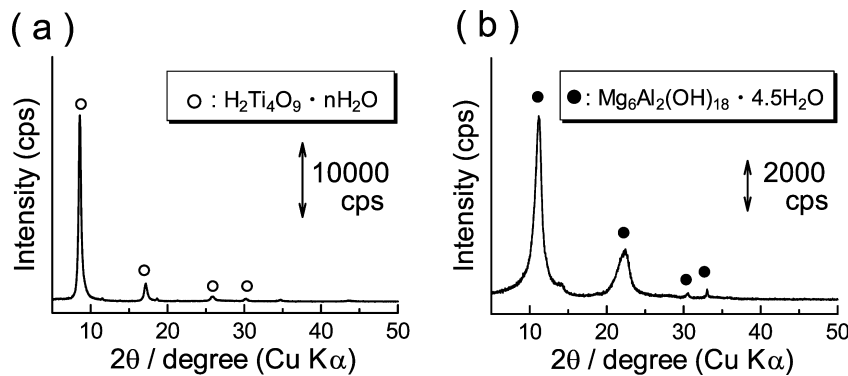


Figure 6. XRD patterns for the (a) HTO and (b) Mg-Al LDH nanosheet films formed by EPD for 100 s under potentiostatic conditions at 7.5 V.

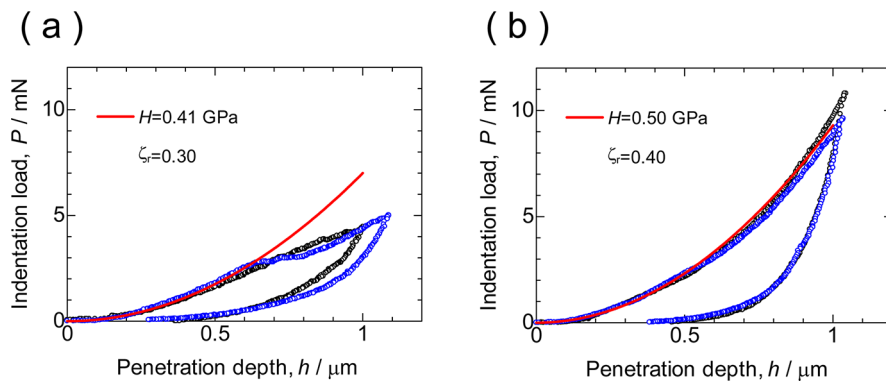


Figure 7. Load–displacement ( $P$ – $h$ ) curves from nanoindentation tests for (a) HTO and (b) Mg-Al LDH nanosheet films. Both films were deposited on ITO-coated glass substrates at 7.5 V for 300 s. The solid curves represent the quadratic relationship between  $P$  and  $h$ .

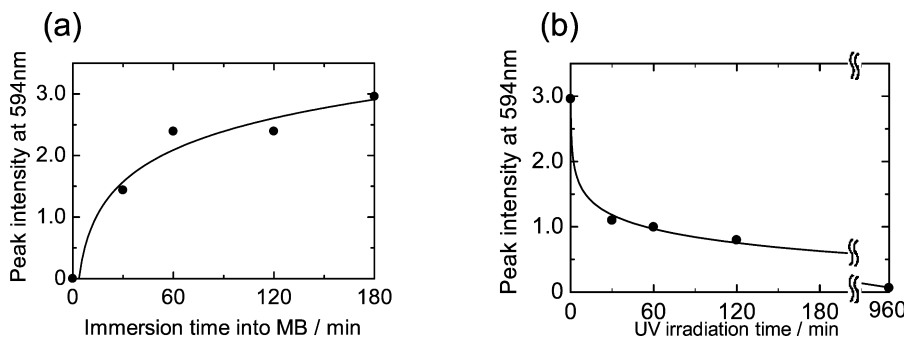


Figure 8. (a) Changes in adsorption behavior of MB into HTO nanosheet films by EPD with soaking time and (b) photobleaching behavior of MB adsorbed by the HTO nanosheet films with UV irradiation time.

( $H_M$ ) was found to be 0.41 and 0.50 GPa for the HTO and LDH films, respectively. These  $H_M$  values are lower than that (5.9 GPa) of SL glass and higher than that (0.28 GPa) of PMMA. The values of the elastoplastic parameter,  $\xi_r$ , as defined in eq 2, were 0.30 and 0.40 for the HTO and LDH films, respectively. These  $\xi_r$  values are smaller than those of SL glass (0.50) and PMMA (0.52), which demonstrates the high elasticity of these EPD nanosheet films with their layered laminate structures. However, the pencil hardness for both the HTO and the LDH films was found to be less than 6 B. This is probably because of the weak adhesion of the laminate nanosheets to the ITO coatings on the glass substrates. It can be expected to improve the adhesion between nanosheets and ITO coatings with a post-annealing.

One attractive feature of the HTO nanosheets is their photocatalytic activity because of their high specific surface area, large adsorption capability, and high protic acidity. Figure

8a and b show the results of adsorption and photobleaching of MB for an HTO film formed by EPD at 7.5 V for 100 s, respectively. The ordinate axes of both graphs indicate the peak intensity at 594 nm of the UV-vis absorption spectra due to MB for the HTO nanosheet film. It is seen from Figure 8a,b that the prepared HTO film shows large MB adsorption and high photocatalytic activity for MB bleaching. The thick HTO nanosheet films are obtained at low temperatures and are, thus, promising for solar cell electrodes and for photocatalytic applications using flexible plastic substrates with low thermal resistance.

High ionic conductivities are expected for the HTO and LDH layered structures because of their high ion exchange capacities. The temperature dependences of the electric conductivities of the EPD films at 80% RH are shown in Figure 9. The open circles and the triangles represent the values for the HTO nanosheet film and the Mg-Al LDH nanosheet

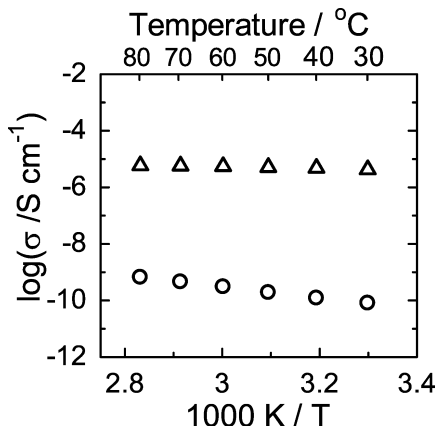


**Figure 9.** Temperature dependence of conductivity under 80% RH for the anionic and cationic nanosheet films obtained by the EPD method. The open circles and open triangles represent the values for the HTO and the Mg-Al LDH nanosheet films, respectively.

film, respectively. The electric conductivities of the HTO nanosheet film and the Mg-Al LDH nanosheet film in the thickness direction were estimated to be  $6.7 \times 10^{-10}$  and  $5.9 \times 10^{-6}$  S/cm at 80 °C, respectively, from impedance analyses. The conductivities of both films increase with increasing temperature, whereas the apparent activation energy of the Mg-Al LDH nanosheet film is smaller than that of the HTO nanosheet film. The relative humidity dependences of the electrical conductivities of the EPD films at 30 °C are shown in Figure 10. The electrical conductivities of both EDP films

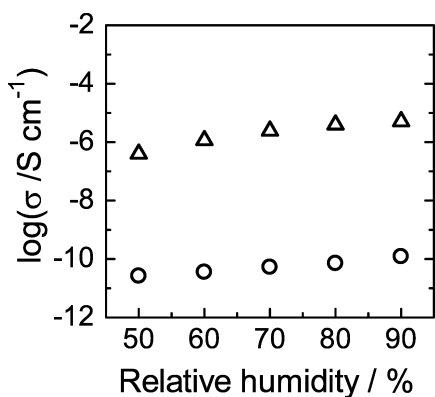


**Figure 10.** Relative humidity dependence of conductivity at 30 °C for the anionic and cationic nanosheet films obtained by the EPD method. The open circles and open triangles have the same meanings as those in Figure 7.

increased with an increase in relative humidity. It is anticipated that the penetration of water molecules between the nanosheets of the EPD films is related to electrical conduction in the EPD films. The  $\text{H}_2\text{Ti}_4\text{O}_9$  nanosheets are composed of corrugated ribbons of edge-sharing  $\text{TiO}_6$  octahedral units, which join at the corners to form stepped sheets separated by  $\text{H}^+$  ions in an intersheet and show protic conduction.<sup>28</sup> The  $[\text{Mg}_{1-x}\text{Al}_x(\text{OH})_2](\text{OH})_x \cdot n\text{H}_2\text{O}$  nanosheets are composed of cationic  $[\text{Mg}_{1-x}\text{Al}_x(\text{OH})_2]^{x+}$  sheets separated by anionic  $[(\text{OH})_x \cdot n\text{H}_2\text{O}]^{x-}$  in an intersheet and exhibit hydroxide conduction.<sup>29</sup> Therefore, in the present study, the conducting ion species are presumed to be the proton ( $\text{H}^+$ ) for the HTO nanosheet film and the hydroxide ion ( $\text{OH}^-$ ) for the Mg-Al

LDH nanosheet film. The ionic conductivity of the pelletized sample of hydrotalcite powder was  $10^{-4}$  S/cm<sup>-1</sup> at 80 °C and 80% RH, which is much higher than that of the ED P LDH film in the thickness direction. The Mg-Al LDH nanosheet films obtained are expected to have anisotropic hydroxide ion conductivity and are useful as solid electrolytes for alkaline-type fuel cells and metal/air batteries when the orientation of the LDH nanosheets in these electrochemical devices is adequately controlled.

## CONCLUSIONS

HTO thick films with layered structures were prepared on positive ITO-coated glass substrates by EPD using anionic  $\text{H}_2\text{Ti}_4\text{O}_9 \cdot n\text{H}_2\text{O}$  nanosheets. The HTO thick films obtained demonstrated high photocatalytic activity, and are promising as photoelectrode materials for solar cells. Mg-Al LDH thick films were also formed on negative ITO-coated glass substrates by EPD using cationic  $\text{Mg}_6\text{Al}_2(\text{OH})_{18} \cdot 4.5\text{H}_2\text{O}$  nanosheets. The Mg-Al LDH thick films showed relatively high ionic conductivity and low activation energy because of their hydroxide ions, and should be useful as a solid electrolyte material for alkaline type fuel cells and metal/air batteries. The EPD films of HTO and Mg-Al LDH nanosheets showed elastic behavior because of their layered laminate structures. The EPD processes of these hydrated oxides and hydroxides are useful for the fabrication of thin film electrochemical devices.

## AUTHOR INFORMATION

### Corresponding Author

\*E-mail: matsuda@ee.tut.ac.jp. Phone: +81 (532) 44 6799. Fax: +81 (532) 48 5833.

### Notes

The authors declare no competing financial interest.

## ACKNOWLEDGMENTS

This work was supported by Grants-in-Aid for Young Scientists (Start-up; Grant No. 21860045) and for Young Scientists (B; Grant No. 22760539). The authors thank Dr. Norio Hakiri of Toyohashi University of Technology for performing the nanoindentation analyses and Mr. Taku Tsuneishi and Mr. Shota Azuma of Toyohashi University of Technology for performing AFM observations and electrochemical analyses.

## REFERENCES

- Corni, I.; Ryan, P. M.; Boccaccini, R. A. *J. Eur. Ceram. Soc.* **2008**, 28, 1353–1367.
- Tada, K.; Onoda, M. *Thin Solid Films* **2003**, 438, 365–368.
- Roether, A. J.; Boccaccini, R. A.; Hench, L. L.; Maquet, V.; Gautier, S.; Jérôme, R. *Biomaterials* **2002**, 23, 3871–3878.
- Schmitt, J.; Decher, G.; Dressick, J. W.; Brandow, L. S.; Geer, E. R.; Shashidhar, R.; Calvart, M. *J. Adv. Mater.* **1997**, 9, 61–65.
- Thomas, C. J. B.; Boccaccini, R. A.; Shaffer, P. S. M. *J. Am. Ceram. Soc.* **2005**, 88, 980–982.
- Sugimoto, W.; Terabayashi, O.; Murakami, Y.; Takasu, Y. *J. Mater. Chem.* **2002**, 12, 3814–3818.
- Gateski, M.; Hwang, S.-J.; Park, H. D.; Ren, Y.; Petkov, V. *Chem. Mater.* **2004**, 16, 5153–5157.
- Iyi, N.; Sasaki, T. *J. Colloid Interface Sci.* **2008**, 322, 237–245.
- Takagaki, A.; Sugisawa, M.; Lu, D.; Kondo, N. J.; Hara, M.; Domen, K.; Hayashi, S. *J. Am. Chem. Soc.* **2003**, 125, 5479–5485.
- Yang, X.; Chen, X.; Yang, L.; Yang, W. *Bioelectrochemistry* **2008**, 74, 90–95.

- (11) Feist, T.; Mocarski, S. L.; Davies, P. K.; Jacobson, A. J.; Lewandowski, J. T. *Solid State Ionics* **1988**, *28*, 1338–1343.
- (12) Sasaki, T.; Komatsu, Y.; Fujiki, Y. *Chem. Mater.* **1992**, *4*, 894–899.
- (13) Sasaki, T.; Watanabe, M.; Michiue, Y.; Komatsu, Y.; Izumi, F.; Takenouchi, S. *Chem. Mater.* **1995**, *7*, 1001–1007.
- (14) Xue, L.; Kajiyoshi, K.; Yan, Y. *Thin Solid Films* **2009**, *518*, 10–15
- (15) Yui, T.; Mori, Y.; Tsuchino, T.; Itoh, T.; Hattori, T.; Fukushima, Y.; Takagi, K. *Chem. Mater.* **2005**, *17*, 206–211.
- (16) Matsuda, A.; Kambayashi, T.; Daiko, Y.; Muto, H.; Sakai, M. *J. Eur. Ceram. Soc.* **2010**, *30*, 1151–1158.
- (17) Aradi, T.; Hornok, V.; Dékány, I. *Colloids Surf., A* **2008**, *319*, 116–121.
- (18) Liu, Z.; Ma, R.; Osada, M.; Iyi, N.; Ebina, Y.; Takada, K.; Sasaki, T. *J. Am. Chem. Soc.* **2006**, *128*, 4872–4880.
- (19) Lee, K.; Nam, J.-D. *J. Power Sources* **2006**, *157*, 201–206.
- (20) Tadanaga, K.; Furukawa, Y.; Hayashi, A.; Tatsumisago, M. *Adv. Mater.* **2010**, *22*, 4401–4404.
- (21) Furukawa, K.; Tadanaga, Y.; Hayashi, A.; Tatsumisago, M. *Solid State Ionics* **2011**, *192*, 185–187.
- (22) He, S.; Zhao, Y.; Wei, M.; Duan, X. *Ind. Eng. Chem. Res.* **2011**, *50*, 2800–2806.
- (23) Lee, J.-H.; Jung, D.-Y. *Chem. Commun.* **2012**, *48*, 5641–5643.
- (24) Sakai, M.; Zhang, J. Q.; Matsuda, A. *J. Mater. Res.* **2005**, *20*, 2173–2183.
- (25) Zhang, J. Q.; Matsuda, A.; Muto, H.; Sakai, M. *Key Eng. Mater.* **2006**, *317* – *318*, 317–322.
- (26) Hakiri, N.; Matsuda, A.; Sakai, M. *J. Mater. Res.* **2009**, *24*, 1950–1959.
- (27) Ainuddin, A. R.; Hakiri, N.; Muto, H.; Sakai, M.; Matsuda, A. *J. Ceram. Soc. Jpn.* **2011**, *119*, 490–493.
- (28) Marani, D.; D'Epifanio, A.; Traversa, E.; Miyayama, M.; Licoccia, S. *Chem. Mater.* **2010**, *22*, 1126–1133.
- (29) Kim, H-S; Yamazaki, Y.; Kim, J-D; Kudo, T.; Honma, I. *Solid State Ionics* **2010**, *181*, 883–888.